A. Colliander, P. Ylä-Oijala, Electromagnetic Scattering from Rough Surface Using Single Integral Equation and Adaptive Integral Method, IEEE Transactions on Antennas and Propagation, vol. 55, no. 12, pp. 3639-3646, December 2007.

Electromagnetic Scattering From Rough Surface Using Single Integral Equation and Adaptive Integral Method

Andreas Colliander, *Member, IEEE*, and Pasi Ylä-Oijala

***Abstract*—An efficient algorithm for electromagnetic wave scattering from rough dielectric surfaces is developed. The algorithm is based on the single magnetic field integral equation (SMFIE) and the surface is discretized using Rao–Wilton–Glisson (RWG) triangular basis functions. The new feature of the algorithm is the application of the adaptive integral method (AIM) with SMFIE for speeding up the calculation. The developed new method utilizes the flexibility of RWG functions to model arbitrary rough surface and the speed of FFT, enabling accurate simulations over large surfaces.**

***Index Terms*—Adaptive integral method (AIM), fast Fourier transform (FFT), Rao–Wilton–Glisson (RWG) triangular basis, rough surface scattering, single magnetic field integral equation (SMFIE).**

I. Introduction

THE simulation of electromagnetic scattering from dielectric rough surfaces is very tempting for applications in remote sensing of ocean, soil and ice. The calculation of full vector-wave scattering from a large surface is very demanding task. The difficulties in the problem lie on the large surface size and on the magnitude of the surface roughness. Solving a problem of this kind requires a lot of unknowns in order to get accurate and meaningful results. Thus, reduction on both computation time and data storage requirement is continuously sought. The surface integral equations are widely used to solve problems of electromagnetic scattering and their formulation is one way to make the simulation more efficient.

There have been two dominating methods for solving a full vector-wave scattering from a two-dimensional (2-D) rough dielectric surface. One of these methods is based on the sparse matrix canonical grid method (SMCG) (e.g., [1]–[3]) and the other is based on the fast multipole method (e.g., [4]–[6]). The SMCG method has also been extended to a three-dimensional (3-D) case, which is called multilevel SMCG [7]. The solution in 3-D allows more accurate results with high magnitude of surface roughness. Both methods distinguish the strong near field interaction and weak far field interaction between field point and source point. This has the advantage that only the near interaction matrix is stored and the far interaction matrix is not stored but its multiplication with a solution vector is calculated by fast means.

The presented technique is based on the single magnetic field integral equation (SMFIE) and the surface is discretized using Rao–Wilton–Glisson (RWG) triangular basis functions [8] to model the rough surface accurately. The SMFIE is demonstrated to be very efficient with iterative solvers [9], [10] and thus is suitable for fast methods. Furthermore, with SMFIE the number of unknowns is reduced to half of the number required by the coupled integral equations (in the case of dielectric scattering; for highly loss scatterers, it is also possible to use a single integral equation with other techniques). The problem with triangular discretization is the fact that the basis functions are not uniformly distributed and the fast Fourier transform (FFT) cannot be directly applied to the matrix-vector multiplication. The adaptive integral method (AIM) solves this by approximating the basis functions on a uniform grid [11]. In general, AIM provides a straightforward and efficient way to speed up the calculation of matrix-vector product. AIM is also significantly less complex than multipole method, or SMCG to some extent. In principle, these methods are optional solutions for rough surface scattering, but beyond this, AIM seems to have wider field of applications.

Although the developed method is applicable to a wide range of practical problems, the main goal of this work is to simulate the bistatic scattering and emission from a large area, with respect to wavelength, of ocean surface. The surface is illuminated with a Gaussian beam so that the borders of the surface do not contribute to the results significantly.

In this paper, Section II presents the formulation of SMFIE and its discretization. Section III presents the application of AIM and FFT, and finally, Section IV presents the simulation results and discussion on the performance of the method.

II. Formulation and Discretization

A. Single Integral Equation Formulation

In this paper a solution to a 3-D time harmonic $(e^{-i\omega t})$ scattering problem from a 2-D dielectric random rough surface is presented. Fig. 1 illustrates the problem. The dielectric medium

Manuscript received November 16, 2006; revised July 8, 2007. This work was supported in part by the Academy of Finland funded EMRES project, by the Graduate School for Remote Sensing (funded by the Academy of Finland and Finnish Ministry of Education) and in part by the Ulla Tuominen, Jenny and Antti Wihuri, Walter Ahlström and Finnish Cultural Foundations.

A. Colliander was with the Laboratory of Space Technology, Helsinki University of Technology, 02150 Espoo, Finland. He is now with the European Research and Technology Centre, European Space Agency, 2200 AG Noordwijk, the Netherlands (e-mail: andreas.colliander@esa.int).

P. Ylä-Oijala is with the Electromagnetics Laboratory, Helsinki University of Technology, FIN-02015 TKK, Finland (e-mail: pasi.yla-oijala@tkk.fi).

Color versions of one or more figures in this paper are available online at http://ieeexplore.ieee.org.

Digital Object Identifier 10.1109/TAP.2007.910337

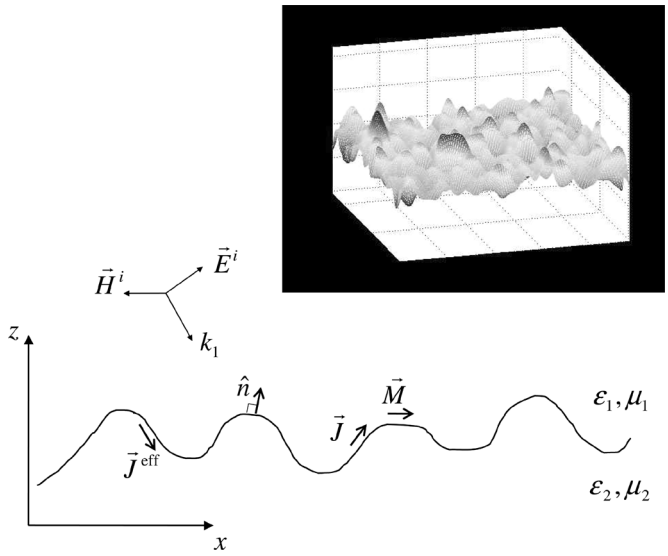

Fig. 1. Schematic diagram of the 3-D scattering problem from a 2-D random rough surface.

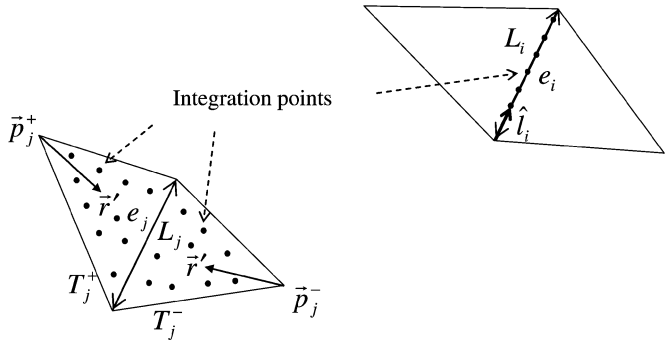

Fig. 2. Triangular RWG function is used as the basis function and the common edge between triangles is used as the testing function. The numerical integration is performed over the surface of the triangles, in the case of the basis function, and along the edge, in the case of the testing function.

over (permittivity ϵ_1, permeability μ_1) and under (ϵ_2, μ_2) the interface is assumed to be homogeneous.

The single integral equation formulation for a closed dielectric object can be described as follows. The fields outside the object are expressed using the usual surface current densities $\vec{J} = \hat{n} \times \vec{H}_1$ and $\vec{M} = -\hat{n} \times \vec{E}_1$, where $\hat{n}$ is the outer unit normal of the object, yielding

$$\vec{E}_1(\vec{r}) = \vec{E}_1^{\text{inc}}(\vec{r}) - \frac{1}{i\omega\epsilon_1}\mathbf{D}_1(\vec{J})(\vec{r}) - \mathbf{K}_1(\vec{M})(\vec{r}) \quad (1)$$

$$\vec{H}_1(\vec{r}) = \vec{H}_1^{\text{inc}}(\vec{r}) - \frac{1}{i\omega\mu_1}\mathbf{D}_1(\vec{M})(\vec{r}) + \mathbf{K}_1(\vec{J})(\vec{r}) \quad (2)$$

where ϵ_1 is the permittivity of the upper medium with $\epsilon_1 = \epsilon_1' + i\sigma_1/\omega$, σ_1 being the conductivity of the medium; ω is the angular frequency and integral operators $\mathbf{D}$ and $\mathbf{K}$ are defined in Appendix I.

Taking the cross product of (2) with the normal vector on the surface, gives the magnetic field integral equation

$$-\frac{1}{i\omega\mu_1}\hat{n} \times \mathbf{D}_1(\vec{M}) + \hat{n} \times \mathbf{K}_1(\vec{J}) - \frac{1}{2}\vec{J} = -\hat{n} \times \vec{H}_1^{\text{inc}}. \quad (3)$$

Inside the object the fields are expressed in terms of an efficient electric current $\vec{J}^{\text{eff}}$ as

$$\vec{E}_2(\vec{r}) = -\frac{1}{i\omega\epsilon_2}\mathbf{D}_2(\vec{J}^{\text{eff}})(\vec{r}) \quad (4)$$

$$\vec{H}_2(\vec{r}) = \mathbf{K}_2(\vec{J}^{\text{eff}})(\vec{r}). \quad (5)$$

The boundary conditions at the interface between the two media

$$\hat{n} \times \vec{E}_1 = \hat{n} \times \vec{E}_2 \quad (6)$$

$$\hat{n} \times \vec{H}_1 = \hat{n} \times \vec{H}_2 \quad (7)$$

give a relation between the currents $\vec{J}, \vec{M}$ and $\vec{J}^{\text{eff}}$ [9]

$$\vec{M} = \frac{1}{i\omega\epsilon_2}\hat{n} \times \mathbf{D}_2(\vec{J}^{\text{eff}}) \quad (8)$$

$$\vec{J} = \hat{n} \times \mathbf{K}_2(\vec{J}^{\text{eff}}) - \frac{1}{2}\vec{J}^{\text{eff}} \quad (9)$$

on the surface S.

Substituting (8) and (9) into (3) gives SMFIE for $\vec{J}^{\text{eff}}$

$$\hat{n} \times \vec{H}_1^{\text{inc}} = \left(\frac{1}{i\omega\mu_1}\frac{1}{i\omega\epsilon_2}\hat{n} \times \mathbf{D}_1(\hat{n} \times \mathbf{D}_2) - \left(\hat{n} \times \mathbf{K}_1 - \frac{1}{2}I\right)\left(\hat{n} \times \mathbf{K}_2 - \frac{1}{2}I\right)\right)(\vec{J}^{\text{eff}}) \quad (10)$$

where I is the identity operator.

Note that SMFIE provides unambiguous solution only outside the resonant frequency of the object and for conducting objects. These requirements are met in the application planned in this study, which is ocean surface.

B. Discretization by the Method of Moments (MoM)

Direct discretization of (10) including products of integral operators with MoM is very ineffective, and, therefore, the discretization is done in two steps using similar technique as in [9].

1) Formulation of System Matrix: The RWG basis functions are used for expanding the currents [8]

$$\vec{f}_j(\vec{r}') = \begin{cases} \frac{L_j}{2A_j^+}(\vec{r}' - \vec{p}_j^{\,+}), & \vec{r}' \in T_j^+ \\ -\frac{L_j}{2A_j^-}(\vec{r}' - \vec{p}_j^{\,-}), & \vec{r}' \in T_j^- \\ 0 & \text{otherwise} \end{cases} \quad (11)$$

where $A_j^{\pm}$ is the area of the triangle $T_j^{\pm}$ and $p_j^{\pm}$ is the vertex of $T_j^{\pm}$ opposite to the common edge. The equations are tested with the following edge functions:

$$\vec{t}_i = \frac{1}{L_i}\hat{l}_i \quad (12)$$

where L_i is the length of edge i and $\hat{l}_i$ is the unit vector of edge i. Fig. 2 shows the principle of the testing and basis functions.

Using the RWG basis functions the effective surface current density can be expressed as

$$\vec{J}^{\text{eff}} = \sum_{i=1}^{N} I_i^{\text{eff}}\vec{f}_i(\vec{r}') \quad (13)$$

where N is the number of interior edges of the mesh and I_i^{eff} are the unknown current coefficients. Similar equation can be written to $\vec{J}$ and I_i^e, and to $\vec{M}$ and I_i^m, respectively.

Using these definitions for basis and testing functions, (3) can be written in matrix form as

$$-\frac{1}{i\omega\mu_1}\bar{\bar{D}}_1\bar{I}^m + \bar{\bar{K}}_1\bar{I}^e = -\bar{b} \tag{14}$$

and (8) and (9) yield

$$\bar{I}^m = -\frac{1}{i\omega\epsilon_2}\bar{\bar{D}}_2\bar{I}^{\text{eff}} \tag{15}$$

$$\bar{I}^e = -\bar{\bar{K}}_2\bar{I}^{\text{eff}} \tag{16}$$

because $\int_{l_i}\vec{t}_i\cdot\vec{f}_j dl = \delta_{ij}$ and thus, the testing procedure yields identity matrices on the left hand sides of the equations. Now, by combining (14)–(16), the SMFIE can be written in matrix form as

$$\left[\frac{1}{i\omega\mu_1}\frac{1}{i\omega\epsilon_2}\bar{\bar{D}}_1\bar{\bar{D}}_2 + \bar{\bar{K}}_1\bar{\bar{K}}_2\right]\bar{I}^{\text{eff}} = \bar{b}. \tag{17}$$

The matrices $\bar{\bar{K}}$ and $\bar{\bar{D}}$ are defined as

$$K_{1,ij} = \frac{1}{L_i}\int_{l_i}\iint_{T_j}(\hat{l}_i\cdot\nabla G_1\times\vec{f}_j)\,ds\,dl - \frac{\Omega_i^-}{2\pi}\delta_{ij} \tag{18}$$

$$\begin{aligned} D_{1,ij} &= k_1^2 V_{1,ij} + W_{1,ij} \qquad (19)\\ &= \frac{1}{L_i}\int_{l_i}\iint_{T_j}\Big[k_1^2(\hat{l}_i\cdot\vec{f}_j)G_1 \\ &\quad +(\hat{l}_i\cdot\nabla G_1)(\nabla_s'\cdot\vec{f}_j)\Big]\,ds\,dl \qquad (20)\end{aligned}$$

where Ω_i^- is the interior angle between triangles at edge i and T_j is both T_j^+ and T_j^- related to the edge j. Note that in the case of the second medium the interior angle is replaced by the exterior angle Ω_i^+. The elements of the excitation vector $\vec{b}$ are

$$b_i = \frac{1}{L_i}\int_{l_i}\hat{l}_i\cdot\hat{n}\times\vec{H}^{\text{inc}}dl \tag{21}$$

which is the average current magnitude flowing across the ith edge.

It should be pointed out that generally a stable discretization of $\bar{\bar{D}}_1\bar{\bar{D}}_2$ requires application of special basis and testing functions [12]. In SMFIE this term is multiplied with $\frac{1}{\omega^2}$ and combined with $(\bar{\bar{K}}_1-\frac{1}{2}I)(\bar{\bar{K}}_2-\frac{1}{2}I)$ resulting accurate results with above discretization when the frequency is high enough.

2) Computation of Far Terms: The elements of the system matrices $\bar{\bar{K}}$ and $\bar{\bar{D}}$, in which the basis and testing function do not have common edges are called here as the far terms. Fig. 2 shows the calculation situation for the far terms; basis function is a triangular RWG function and the testing function is an edge between two RWG triangles. The calculation is a straightforward process of applying standard numerical integration on the triangles and the line.

3) Computation of Near Terms: The elements of the system matrices $\bar{\bar{K}}$ and $\bar{\bar{D}}$, in which the basis and testing function has common edges are called here as the near terms. The obvious case for the near terms is when $i = j$, but there is also cases when an edge or vertex of a testing function is one of the edges or vertices of a basis function.

When $i = j$, the first term of $\bar{\bar{K}}$ vanishes and the elements are calculated simply by solving the angle between the triangles. However, elements of $\bar{\bar{V}}$ and $\bar{\bar{W}}$ withhold a singularity, which is solved, in the first case, using a transformation to the polar coordinates, and in the latter case, using Gauss divergence theorem.

The transformation to the polar coordinates is done so that the singularity is located in the origin dividing the RWG triangle into two subtriangles. This eliminates the problem, since the singularity is of order $\sim(1/r)$ [14].

For $\bar{\bar{W}}$, the Gauss divergence theorem can be applied to transform the surface integral to a boundary integral. The benefit of this treatment is the fact that the dot product of the outer normal of the edge withholding the singularity and the testing function yields zero. See Appendix II for a detailed explanation of the method. Note that, e.g., in [7], [9], and [10] this term is not calculated with this kind of precision.

When $i \neq j$, but the edge of the testing function is one of the edges of the basis function these same methods are applied, including the elements of $\bar{\bar{K}}$, to which the Gauss divergence theorem is used (see Appendix II). And when $i \neq j$, but the vertices of the basis and the testing function are the same, the integration points are located so that the effect of the singularity is damped.

C. Application To Rough Surface Scattering

The above treatment is made for a closed object. The simulation of surface scattering has the problem that the surface is very large and it is more practical to model it as an open surface than a closed object. Hence, the effect of the borders of the surface need to be minimized. Fig. 3 shows a calculation where the scattering from a closed object (box of size $n\lambda\times n\lambda\times\lambda/10$, where λ is the free space wavelength) is compared to the scattering from a plate (of size $n\lambda\times n\lambda$) in order to evaluate the effect of the truncation of the surface to a finite size. The surfaces are flat and the properties of the surfaces are the same as in the examples in Figs. 6, 7 and 8. The results show that the truncation has no critical effect on the result. This is related to the relative large conductivity of the surface, which attenuates the incident field toward the borders of the surface area. The large conductivity originates from the fact that the aim of the study is to simulate scattering from ocean surface.

Furthermore, a common technique is applied in which an incident field with amplitude tapering toward the edges of the surface is used. In the simulations of this study the field presented in [16] has been used. The x-component of magnetic field is Gaussian tapered and the y-component is zero, i.e., [16]

$$H_x^{\text{inc}} = -\frac{1}{\eta_0}e^{-(x^2+y^2)/g^2} \tag{22}$$

where g is the parameter that defines the tapering of the field amplitude on the surface.

III. Application of AIM and FFT

To decrease computational complicity of the method, FFT in 2-D is applied. In order to solve a scattering problem using FFT the surface must be divided into a uniform grid,

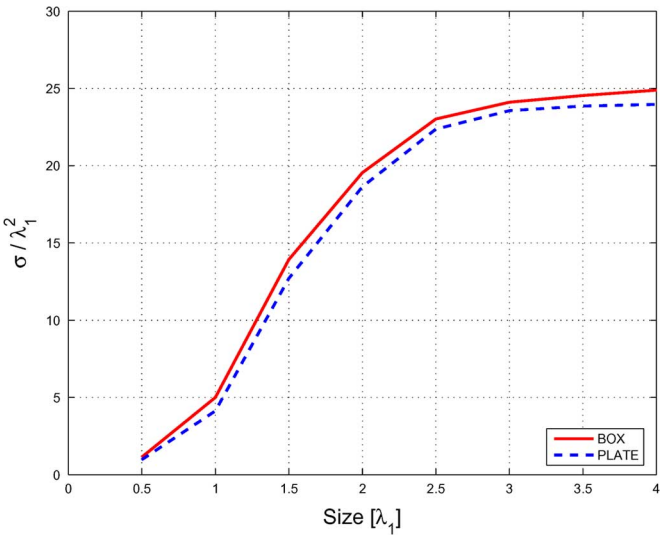

Fig. 3. Backscattered RCS (in units of λ^2) of a dielectric box (box) with thickness $\lambda_1/10$ and of a thin box (plate) thin zero thickness corresponding to a truncated surface. Horizontal axis gives the size of the box in terms of λ_1.

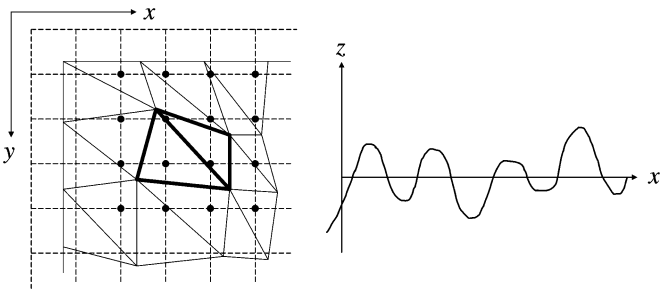

Fig. 4. Piece of the surface divided into triangle shaped patches and the grid for AIM. The dots indicate the grid points for which the coefficients are solved in order to determine the translated basis function of the highlighted RWG-basis function.

which is not the case when RWG basis functions are applied. However, the RWG basis functions can be translated to a functions of a uniform grid using AIM [11]. This approach utilizes the benefits of RWG basis functions [8] and speed of FFT. Conventionally, AIM is applied to a discretization using Galerkin method. Here, AIM is applied on the discretization with different basis and testing functions, which, however, does not cause any extra issues. Nevertheless, this formulation is presented explicitly.

A. Basic Idea of AIM

Fig. 4 shows a schematic diagram of a piece of a surface. The rectangular grid is the grid laid out for the AIM, and the triangles denote the actual surface discretized using triangular RWG basis functions. The height of the surface varies in z-direction. The AIM grid is positioned at z axis so that it is at the mean level of the surface height.

The idea of the AIM is as follows [11], [13]: consider matrix element of MoM equation with a basis function ψ_j and a testing function φ_i having the following form:

$$z_{ij} = \int_{l_i} \iint_{T_j} \psi_j(\vec{r}) G(\vec{r}, \vec{r}') \varphi_i(\vec{r}') ds'\, dl \tag{23}$$

where G is the Green's function. The basis and testing functions can be translated from a triangular grid onto a uniform rectangular grid by approximating them with a combination of the Dirac delta functions on a rectangular grid as follows:

$$\psi_j(\vec{r}) \approx \hat{\psi}_j(\vec{r}) = \sum_{u=1}^{(M+1)^2} Q_{ju} \delta(\vec{r} - \vec{r}_u) \tag{24}$$

where Q_{ju} is the expansion coefficient for the basis function $\psi_j(\vec{r})$, M is the expansion order and $\vec{r}_u$ is the vector for the grid location. The matrix element z_{ij} can now be approximated with the translated basis and testing functions, Q_j and U_i, as follows:

$$\hat{z}_{ij} = \sum_{u=1}^{(M+1)^2} \sum_{v=1}^{(M+1)^2} Q_{ju} G(\vec{r}_u, \vec{r}_v) U_{iv} \tag{25}$$

to which FFT can be applied due to the uniform distribution of calculation points along the geometry.

One way of solving the translated functions is based on the multipole moment approximation. The goal is that the translated function produces the same multipole moments as those of the original basis (or testing) function. This can be solved from the following [13]:

$$\sum_{u=1}^{(M+1)^2} (x_u - x_0)^{q_1} (y_u - y_0)^{q_2} Q_{ju} = \iint_S \psi_j(\vec{r}) (x - x_0)^{q_1} (y - y_0)^{q_2} dS \qquad 0 \le q_1, q_2 \le M \tag{26}$$

where the reference point $\vec{r}_0 = (x_0, y_0)$ is chosen as the center of the basis (or testing) function. Note that this approach does not directly apply to the matrices $\bar{\bar{W}}$ and $\bar{\bar{K}}$ including the derivatives of the Green's function. Application of AIM to these terms is considered in next.

In Fig. 4, the dots indicate the grid points for which the coefficients are solved in order to determine the translated function of the highlighted RWG-basis function. In the case of the figure, $M = 3$ yielding 16 coefficients for each translated function. Note also that AIM can be applied only to the far interaction terms and the near terms have to be calculated with standard MoM.

B. AIM for SMFIE

The FFT is used to speed up the matrix-vector products of (17). Two operators are defined in order to solve these products with FFT: $\mathcal{K}^{\mathcal{F}}_{1/2}$ and $\mathcal{D}^{\mathcal{F}}_{1/2}$, where $\mathcal{K}^{\mathcal{F}}_{1/2}(\bar{X})$ and $\mathcal{D}^{\mathcal{F}}_{1/2}(\bar{X})$ denote calculation of the matrix-vector products $\bar{\bar{K}}_{1/2}\bar{X}$ and $\bar{\bar{D}}_{1/2}\bar{X}$, respectively, with FFT.

$\mathcal{K}_2^{\mathcal{F}}(\bar{X})$ is defined by the subsequent operations. First, the vector potential is computed with FFT

$$\bar{A}_{2x} = \mathcal{F}^{-1}\{\mathcal{F}\{\bar{G}_2\} \cdot \mathcal{F}\{\bar{\bar{Q}}_x \bar{X}\}\} \tag{27}$$
$$\bar{A}_{2y} = \mathcal{F}^{-1}\{\mathcal{F}\{\bar{G}_2\} \cdot \mathcal{F}\{\bar{\bar{Q}}_y \bar{X}\}\} \tag{28}$$
$$\bar{A}_{2z} = \mathcal{F}^{-1}\{\mathcal{F}\{\bar{G}_2\} \cdot \mathcal{F}\{\bar{\bar{Q}}_z \bar{X}\}\} \tag{29}$$

where $\bar{G}_2$ is a $\Pi \times 1$ vector of Green's function of AIM grid of size $\Pi \times \Pi$, $\bar{\bar{Q}}_{x,y,z}$ is a $\Pi \times N$ matrix of AIM coefficients of the x, y and z components of the basis functions and $\bar{X}$ is a $N \times 1$ vector. The curl of the vector potential is then defined as

$$\vec{A}_2{}' = \nabla \times \vec{A}_2 = \left(\frac{\partial A_{2z}}{\partial y} - \frac{\partial A_{2y}}{\partial z}\right)\hat{x} + \left(\frac{\partial A_{2x}}{\partial z} - \frac{\partial A_{2z}}{\partial x}\right)\hat{y} + \left(\frac{\partial A_{2y}}{\partial x} - \frac{\partial A_{2x}}{\partial y}\right)\hat{z} \tag{30}$$

where x- and y-components yield zero in a 2-D AIM grid. The z-component is solved numerically using the points of the AIM grid (approach adopted from [15])

$$\frac{\partial A_{2y}}{\partial x} = \frac{A_{2y}^{(n+1)} - A_{2y}^{(n-1)}}{2\Delta x} \tag{31}$$
$$\frac{\partial A_{2x}}{\partial y} = \frac{A_{2x}^{(n+1)} - A_{2x}^{(n-1)}}{2\Delta y}. \tag{32}$$

At the edge of the area the gradient is calculated between the adjacent points, i.e., with spacing Δx or Δy.

Finally, the operations are completed with multiplication by AIM-coefficients of the z-component of the testing function, yielding

$$\mathcal{K}_2^{\mathcal{F}}(\bar{X}) = \bar{\bar{U}}_z \bar{A}'_{2z} + \bar{\bar{K}}_2^{\Delta} \bar{X} \tag{33}$$

where K_2^{Δ} is the difference of the strong interaction elements between MoM and AIM solution of $\bar{\bar{K}}_2$ in the lower medium, i.e.

$$K_{2,ij}^{\Delta} = K_{2,ij}^{\mathrm{AIM}} - K_{2,ij}. \tag{34}$$

$\mathcal{D}_2^{\mathcal{F}}(\bar{X})$ is defined by the subsequent operations. First, the vector potential is solved with FFT

$$\bar{v}_{2x} = \mathcal{F}^{-1}\{\mathcal{F}\{\bar{G}_2\} \cdot \mathcal{F}\{\bar{\bar{Q}}_x \bar{X}\}\} \tag{35}$$
$$\bar{v}_{2y} = \mathcal{F}^{-1}\{\mathcal{F}\{\bar{G}_2\} \cdot \mathcal{F}\{\bar{\bar{Q}}_y \bar{X}\}\} \tag{36}$$
$$\bar{v}_{2z} = \mathcal{F}^{-1}\{\mathcal{F}\{\bar{G}_2\} \cdot \mathcal{F}\{\bar{\bar{Q}}_z \bar{X}\}\} \tag{37}$$

which is then multiplied with the testing function, i.e., the AIM-coefficients of the testing function

$$\bar{\bar{V}}_2 \bar{X} = \bar{\bar{U}}_x \bar{v}_{2x} + \bar{\bar{U}}_y \bar{v}_{2y} + \bar{\bar{U}}_z \bar{v}_{2z}. \tag{38}$$

For clarity, this outcome would correspond to $\bar{\bar{V}}_2 \bar{I}^{\mathrm{eff}}$.

In order to solve the correspondence of $\bar{\bar{W}}_2 \bar{I}^{\mathrm{eff}}$ the following multiplication is performed:

$$\bar{w}_2 = -\mathcal{F}^{-1}\{\mathcal{F}\{\bar{G}_2\} \cdot \mathcal{F}\{\bar{\bar{Q}}_d \bar{X}\}\} \tag{39}$$

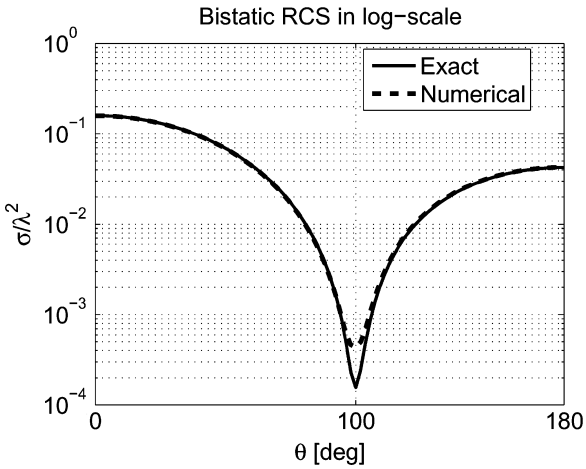

Fig. 5. Bistatic RCS (in units of λ^2) of a dielectric sphere with $\epsilon_{r2} = 4$.

where $\bar{\bar{Q}}_d$ is the AIM coefficients of the surface divergence of the basis function. Next, the gradient of w_2 is solved

$$\bar{w}_2' = \nabla \bar{w}_2 = \frac{\partial \bar{w}_2}{\partial x}\hat{x} + \frac{\partial \bar{w}_2}{\partial y}\hat{y} + \frac{\partial \bar{w}_2}{\partial z}\hat{z} \tag{40}$$

where z-component equals zero. The partial differences are solved numerically as in (31), and the result is multiplied with the AIM-coefficients of the testing function

$$\bar{\bar{W}}_2 \bar{X} = \bar{\bar{U}}_x \bar{w}'_{2x} + \bar{\bar{U}}_y \bar{w}'_{2y}. \tag{41}$$

Now, the outcome of the operator can be written as

$$\mathcal{D}_2^{\mathcal{F}}(\bar{X}) = k_2^2 \bar{\bar{V}}_2 \bar{X} + \bar{\bar{W}}_2 \bar{X} + D_2^{\Delta} \bar{X} \tag{42}$$

where D_2^{Δ} is the difference of the strong interaction elements between MoM and AIM solutions of $\bar{\bar{D}}_2$.

With the above treatment the system matrix multiplication takes the form, see (17)

$$A(I^{\mathrm{eff}}) = \frac{1}{\omega^2 \mu_1 \epsilon_2} \mathcal{D}_1^{\mathcal{F}}\left(\mathcal{D}_2^{\mathcal{F}}(I^{\mathrm{eff}})\right) + \mathcal{K}_1^{\mathcal{F}}\left(\mathcal{K}_2^{\mathcal{F}}(I^{\mathrm{eff}})\right) \tag{43}$$

which yields the following equation for the iteration process:

$$A(I^{\mathrm{eff}}) = \bar{b} \tag{44}$$

where $\bar{b}$ is the excitation vector.

IV. Simulation Results

A. Demonstration With Sphere

The formulation was verified by computing the radar cross section (RCS) of a sphere and comparing that to the exact solution of RCS of the sphere. Fig. 5 shows both the exact and the numerical solution. The radius of the sphere is 0.5 m, relative permittivity $\epsilon_{r2} = 4$ and frequency 100 MHz. The sphere was illuminated with the plane wave travelling to the direction of z axis. The electric field of the plane wave was in the direction of the y axis and the result is plotted in the yz plane. The exact

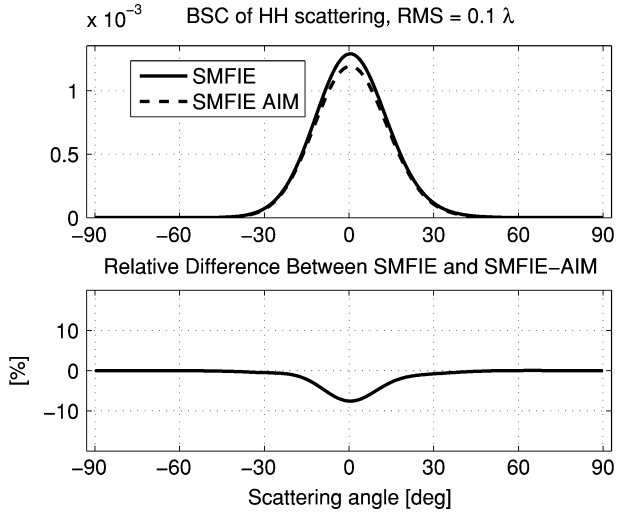

Fig. 6. BSC of averaged HH scattering from ten realizations of surfaces with 0.1λ RMS roughness and 1λ correlation length. The size of the surface is $16\lambda^2$ and the surface is illuminated from the nadir direction.

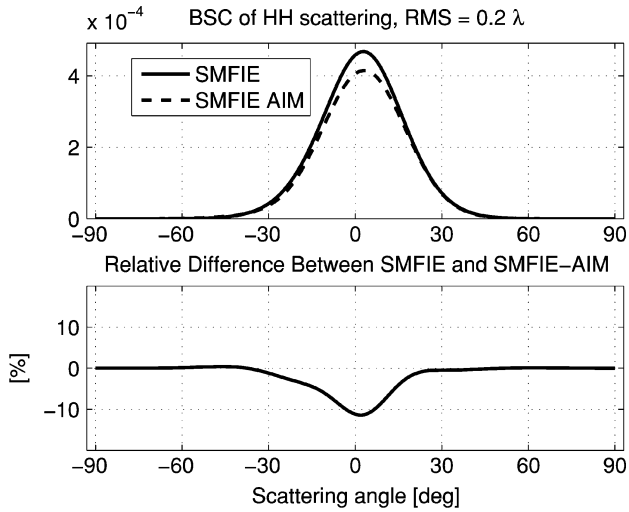

Fig. 7. BSC of averaged HH scattering from ten realizations of surfaces with 0.2λ RMS roughness and 1λ correlation length. The size of the surface is $16\lambda^2$ and the surface is illuminated from the nadir direction.

and numerical solution coincide accurately. The difference at the minimum is due to the discretization of the ball, which was divided into only 960 RWG basis functions.

B. Bistatic Scattering Coefficients

Bistatic scattering coefficients (BSC) were simulated with the presented method. Figs. 6 and 7 show the averaged scattering results in terms of BSC for the cases where the RMS roughnesses of ten realizations of surfaces are 0.1 and 0.2 wavelengths, respectively. The surfaces were created following the principles presented in [17]. The frequency in the calculation was 14 GHz and the relative permittivity of the lower medium is $\epsilon_{r2} = 39.7 + i40.2$. The size of the surface is $16\lambda^2$, which is divided into 2133 edges of RWG basis functions. The surface was illuminated from the nadir direction with a Gaussian tapered beam as described in Section II.

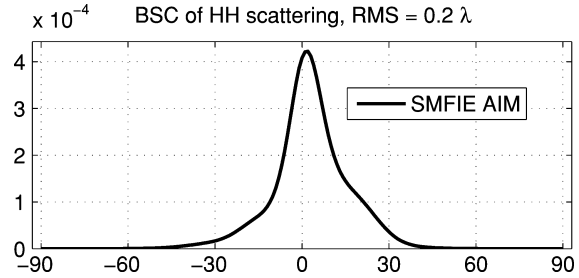

Fig. 8. BSC of averaged HH scattering from ten realizations of surfaces with 0.2λ RMS roughness and 1λ correlation length. The size of the surface is $100\lambda^2$, and the surface is illuminated from the nadir direction.

In order to solve the scattering using the AIM a 14 by 14 grid was laid out onto the level of the mean of the surface height. The grid extends over the surface borders in x- and y-directions in order to allow the determination of the translated functions for the original functions also on the borders of the surface. The translated functions were combinations of 16 coefficients $(M = 3)$. In Fig. 7 the maximum does not point exactly to the nadir, which is due to the fact that the beam was narrow on the surface with respect to the correlation length of the surface. The result show that as the roughness increases the difference between solution using only SMFIE and the solution using SMFIE with AIM increases. This is clearly due to the fact that the AIM coefficients are evaluated on the xy plane and as the roughness increases the distance of these points to the actual surface points increases causing uncertainty.

Fig. 8 shows averaged scattering in terms of BSC from ten realizations of $100\lambda^2$ surfaces, which were divided into 18 565 edges of RWG basis functions. The surface roughness was 0.2λ RMS and the correlation length 1λ. The shape of the scattering pattern is narrower than the one observed in Fig. 7 (same roughness). This is due to the fact that as a larger surface area is illuminated, the main lobe of scattering is narrower having sidelobes with more random amplitude and phase in each scattering realization. The presented result show the feasibility of the method to solve scattering from large surface areas.

All results were obtained with very modest computational power; standard PC computers with one gigabyte of memory. With AIM, the computation time grows as $N \log N$ and the memory requirement as N, where N is the number of unknowns [18]. This represents state-of-the-art performance. The accuracy compares well to other presented methods, although reports on precise accuracy values are hard to find. It is noted that an error of 10% corresponds to 0.5 dB, which commonly goes even undetected due to the use of decibel-plots.

C. Convergence Speed

The results were calculated using generalized minimum residual method (GMRES) without preconditioner or restart. The convergence speed of GMRES for the SMFIE solution was also studied since it was indicated in [9] that the SMFIE should perform very efficiently with iterative methods. In the abovementioned cases the solution (to the accuracy of 10^{-6}) was found in 7 to 11 iterations, including the solutions to scattering from the larger surfaces. Hence, the efficiency of

the SMFIE is regarded excellent and SMFIE formulation very suitable for solving this kind of problems.

V. Conclusion

The SMFIE formulation using AIM for solving the scattering problem of a rough dielectric surface with MoM was presented. The SMFIE implementation was verified by calculating the bistatic RCS of a sphere. The rough surface scattering was simulated by calculating the BSC for two surfaces with different roughnesses with and without application of AIM. Also, the result for a very large surface was demonstrated.

It is concluded that the combination of SMFIE, RWG functions, and AIM is a good basis for flexible and accurate modeling of the surface, imposes fast solving with FFT and less unknowns (compared to coupled integral equations), and enables efficient simulation of large surfaces. However, as the roughness of the surface increases the accuracy of the solution using AIM decreases, which has the consequence that in order to use this approach to the simulation of scattering from extremely rough surface an improvement is needed to take the height variations of the surface into account.

Appendix I

Here, the definition of the integral operators is given. The integral operators $\mathbf{K}_l$ and $\mathbf{D}_l$ are defined as $(l = 1, 2)$

$$\mathbf{K}_l(\vec{F})(\vec{r}) = \int_S \nabla G_l(\vec{r},\vec{r}\,') \times \vec{F}(\vec{r}\,')dS' \tag{45}$$

$$\mathbf{D}_l(\vec{F})(\vec{r}) = k_l^2 \int_S G_l(\vec{r},\vec{r}\,')\vec{F}(\vec{r}\,')dS' + \nabla \int_S G_l(\vec{r},\vec{r}\,')\nabla'_s \cdot \vec{F}(\vec{r}\,')dS' \tag{46}$$

where

$$G_l = \frac{e^{ik_l|\vec{r}-\vec{r}\,'|}}{4\pi|\vec{r}-\vec{r}\,'|} \tag{47}$$

is the homogeneous space Green's function of domain D (so that $\vec{r}$ is the location where the field is evaluated due to the current distribution at $\vec{r}\,'$ and $k_l = \omega\sqrt{\mu_l\epsilon_l}$ is the wavenumber) and $\nabla'_s\cdot$ denotes the surface divergences with respect to the primed coordinates.

Appendix II

Here, the application of the Gauss divergence theorem in order to avoid the integration over the singularity is introduced. The Gauss divergence theorem can be used to transform the surface integral to a boundary integral, which eliminates the integration over the singularity for the near terms of $\bar{\bar{W}}$, as is shown next.

Writing only the essential part of an element of $\bar{\bar{W}}$ and dividing it into tangential and normal components yields

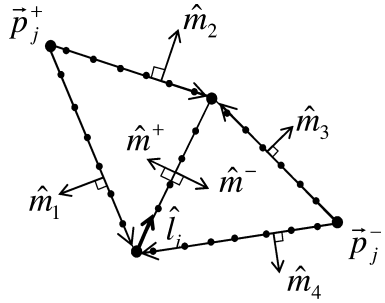

Fig. 9. Integration of an element of $\bar{\bar{W}}$, which has the same basis and testing function. The integration over the singularity is overcome by applying Gauss divergence theorem.

(see Fig. 9)

$$\int_{l_i}\int_{T_j} \nabla G_1 \cdot \hat{l}_i \, ds\, dl = \int_{l_i}\int_{T_j} (\nabla_T + \nabla_N) G_1 \cdot \hat{l}_i \, ds\, dl. \tag{48}$$

Since the normal component of the two triangles and the direction of the edge are perpendicular to each other, the normal component vanishes. Now, by applying the Gauss divergence theorem gives:

$$\begin{aligned}\int_{l_i}\int_{T_j} \nabla_T G_1 \cdot \hat{l}_i \, ds\, dl &= -\int_{l_i}\oint_{C_j} G_1(\hat{l}_i \cdot \hat{m}_j)\, dc\, dl \\ &= -\int_{l_i}\sum_{q=1}^{4}\oint_{C_j^q} G_1(\hat{l}_i \cdot \hat{m}_j^q)\, dc\, dl\end{aligned} \tag{49}$$

where $\hat{m}_j^q$ is a unit vector of the outer normal of the boundary C_j^q of jth basis function (see Fig. 9). The singularity withholding edge is left out, since

$$\hat{m}^+ \cdot \hat{l}_i = \hat{m}^- \cdot \hat{l}_i = 0 \tag{50}$$

as is evident from Fig. 9. This way the integration of this terms becomes very accurate.

When the edge of the testing function is one of the other edges of the triangles of an RWG basis function, the method can also be applied to the elements of $\bar{\bar{K}}$. In this case, the tangential component of the triangle vanishes directly, and the normal component through the Gauss theorem, since $\hat{l} \times \vec{f}$ is in the direction of the normal of the triangle. This way the integral over the triangle, where the testing edge resides, vanishes altogether.

Acknowledgment

Profs. J. Sarvas from Helsinki University of Technology and J. Pulliainen from the Finnish Meteorological Institute are acknowledged for advisory in the frame of the Electromagnetic Modeling of the Earth's Surface and Atmospheric Targets for Microwave Remote Sensing (EMRES) project.

REFERENCES

[1] L. Tsang, C. H. Chan, and K. Pak, "Monte Carlo simulation of large-scale problems of random rough surface scattering and applications to grazing incidence with the BMIA/canonical grid method," *IEEE Trans. Antennas Propag.*, vol. 43, pp. 851–859, Aug. 1995.

[2] K. Pak, L. Tsang, and J. T. Johnson, "Numerical simulations and backscattering enhancement of electromagnetic waves from two-dimensional dielectric random rough surfaces with the sparse-matrix canonical grid method," *J. Opt. Soc. Amer. A*, vol. 14, no. 7, pp. 1515–1529, Jul. 1997.

[3] L. Zhou, L. Tsang, V. Janshyala, Q. Li, and C. H. Chan, "Emissivity simulations in passice microwave remote sensing with 3-D numerical solutions of Maxwell equations," *IEEE Trans. Geosci. Remote Sens.*, vol. 42, no. 8, Aug. 2004.

[4] R. L. Wagner, J. Song, and W. C. Chew, "Monte Carlo simulation of electromagnetic scattering from two-dimensional random rough surface," *IEEE Trans. Antennas Propag.*, vol. 45, pp. 235–245, Jan. 1997.

[5] P. Wang, M. Y. Xia, and L. Z. Zhou, "Analysis of scattering by composite conducting and dielectric bodies using the single integral equation method and multilevel fast multipole algorithm," *Microw. Opt. Technol. Lett.*, vol. 48, no. 6, pp. 1055–1059, Jun. 2006.

[6] Y. Juan, B. Shanker, and L. C. Kempel, "Fast multipole augmented analysis of scattering from dielectric objects using the single integral equation," in *20th Ann. Rev. Progress in Appl. Computat. Electromagn.*, Syracuse, NY, Apr. 19–23, 2004.

[7] M. Y. Xia, C. H. Chan, S. Q. Li, B. Zhang, and L. Tsang, "An efficient algorithm for electromagnetic scattering from rough surfaces using a single integral equation and multilevel sparse-matrix canonical-grid method," *IEEE Trans. Antennas Propag.*, vol. 51, no. 6, pp. 1142–1149, Jun. 2003.

[8] S. M. Rao, D. R. Wilton, and A. W. Glisson, "Electromagnetic scattering by surfaces of arbitrary shape," *IEEE Trans. Antennas Propag.*, vol. AP-30, no. 3, pp. 409–418, May 1982.

[9] M. S. Yeung, "Single integral equation for electromagnetic scattering by three-dimensional homogeneous dielectric objects," *IEEE Trans. Antennas Propag.*, vol. 47, no. 10, pp. 1615–1622, Oct. 1999.

[10] M. S. Yeung, "Solution of electromagnetic scattering problems involving three dimensional homogeneous dielectric objects by the single integral equation method," *SIAM J. Scientif. Comput.*, vol. 15, no. 1, pp. 1–17, 2000.

[11] E. Bleszynski, M. Bleszynski, and T. Jaroszewicz, "AIM: Adaptive integral method for solving large-scale electromagnetic scattering and radiation problems," *Radio Sci.*, vol. 31, pp. 1225–1251, Sep.–Oct. 1996.

[12] R. J. Adams and N. J. Champagne, II, "A numerical implementation of a modified form of the electric field integral equation," *IEEE Trans. Antennas Propag.*, vol. 52, no. 9, pp. 2262–2266, Sep. 2004.

[13] J. Jin, *The Finite Element Method in Electromagnetics*, 2nd ed. New York: Wiley, 2002.

[14] C. Schwab and W. L. Wendland, "On numerical cubatures of singular surface integrals in boundary element methods," *Numerische Mathematik*, vol. 62, pp. 343–369, 1992.

[15] X.-C. Nie, L.-W. Li, and N. Yuan, "Precorrected-FFT algorithm for solving combined field integral equations in electromagnetic scattering," *J. Electromagn. Waves Appl.*, vol. 16, no. 8, pp. 1171–1187, 2002.

[16] J. T. Johnson, R. T. Shin, J. A. Kong, L. Tsang, and K. Pak, "A numerical study of ocean polarimetric thermal emission," *IEEE Trans. Geosci. Remote Sens.*, vol. 37, no. 1, pp. 8–20, Jan. 1999.

[17] S. C. Wu, M. F. Chen, and A. K. Fung, "Non-Gaussian surface generation," *IEEE Trans. Geosci. Remote Sens.*, vol. 26, no. 6, Nov. 1988.

[18] F. Ling, C. F. Wang, and J. M. Jin, "Application of adaptive integral method to scattering and radiation analysis of arbitrarily shaped planar structures," *J. Electromagn. Waves Appl.*, vol. 12, pp. 1021–1038, Aug. 1998.

Andreas Colliander (S'04–A'06–M'07) was born in Imatra, Finland, in 1976. He received the M.Sc. (Tech.), Lic.Sc. (Tech.), and D.Sc. (Tech.) degrees from Helsinki University of Technology (TKK), Espoo, Finland, in 2002, 2005, and 2007, respectively.

He is currently with the European Space Agency's (ESA) European Space Research and Technology Centre (ESTEC) as a Research Fellow. From 2001 to 2007, he was with the Laboratory of Space Technology, TKK, where he worked as a Research Scientist and Project Manager. His research is focused on microwave radiometry, with emphasis on polarimetric and interferometric radiometer systems, and on theoretical simulation of rough-surface backscattering. He has authored or coauthored over 30 scientific publications on microwave remote sensing.

Mr. Colliander was a recipient of the TKK Master's Thesis Award, an annual award for the top five Master's thesis of TKK.

Pasi Ylä-Oijala received the M.Sc. and Ph.D. degrees in applied mathematics from the University of Helsinki, Helsinki, Finland, in 1992 and 1999, respectively.

Currently, he is a Finnish Academy Research Fellow with the Electromagnetics Laboratory, Helsinki University of Technology, Espoo, Finland. His field of interest includes integral equation and fast methods in computational electromagnetics.